Analytic continuation of the self-energy via Machine Learning techniques

Taegeun Song,[1, 2] Roser Valentí,[3] and Hunpyo Lee[4, *]

[1]*Department of Physics, Pohang University of Science and Technology, Pohang 37673, Republic of Korea*
[2]*The Abdus Salam International Centre for Theoretical Physics (ICTP), Strada Costiera 11, I-34151 Trieste, Italy*
[3]*Institute of Theoretical Physics, Goethe University Frankfurt,*
Max-von-Laue-Strasse 1, 60438 Frankfurt am Main, Germany
[4]*School of Liberal Studies, Kangwon National University, Samcheok, 25913, Republic of Korea*
(Dated: July 28, 2020)

We develop a novel analytic continuation method for self-energies on the Matsubara domain as computed by quantum Monte Carlo simulations within dynamical mean field theory (QMC+DMFT). Unlike a maximum entropy (maxEn) procedure employed for the last thirty years, our approach is based on a machine learning (ML) technique in combination with the iterative perturbative theory impurity solver of the dynamical mean field theory self-consistent process (IPT+DMFT). The input and output training datasets for ML are simultaneously obtained from IPT+DMFT calculations on Matsubara and real frequency domains, respectively. The QMC+DMFT self-energy on real frequencies is determined from the -usually noisy- input QMC+DMFT self-energy on the Matsubara domain and the trained ML kernel. Our approach is free from both, bias of ML training datasets and from fitting parameters present in the maxEn method. We demonstrate the efficiency of the method on the testbed frustrated Hubbard model on the square lattice.

Introduction.- Electronic properties in strongly correlated systems have been intensively studied within the dynamical mean field theory (DMFT) approximation [1–5] by making use of powerful quantum Monte Carlo (QMC+DMFT) methods as impurity solvers [6–10]. While QMC+DMFT has successfully accounted for a variety of phases such as Fermi-liquid, non-Fermi-liquid and paramagnetic Mott insulator, to mention a few, the calculated impurity Green's functions $G_\sigma(i\omega_n)$ (or self-energy $\Sigma_\sigma(i\omega_n)$) with spin index σ, retain numerical noise in the Matsubara domain $(i\omega_n)$ [6–8]. This noise creates unfortunately large uncertainties in the results of $G_\sigma(\omega)$ after performing analytic continuation to real frequencies ω with the methods presently at hand.

The most widely employed tool for analytic continuation of $G_\sigma(i\omega_n)$ is the maximum entropy (maxEn) method [11]. This technique is based on defining a goodness-of-fit functional χ^2 and entropy S associated with the spectral function $A_\sigma(\omega) = \frac{1}{\pi}\mathrm{Im}G_\sigma(\omega + i0^+)$. The optimized solution is then determined by minimizing $F(\alpha) = \chi^2 - \alpha^{-1}S$ where α is a parameter which controls the degree of regularization. However, the results of the maxEn analytic continuation are strongly dependent on α [12]. Furthermore, for a direct comparison to experimental observations, analytic continuation of the self-energy $\Sigma_\sigma^{\mathrm{QMC+DMFT}}(i\omega_n)$ calculated within DMFT+QMC is required. The uncertainty in the analytic continuation of $\Sigma_\sigma^{\mathrm{QMC+DMFT}}(i\omega_n)$ is much larger than that of $G_\sigma^{\mathrm{QMC+DMFT}}(i\omega_n)$, due to the inversion problem of $G_\sigma^{\mathrm{QMC+DMFT}}(i\omega_n)$ in the Dyson's equation [12]. Therefore, for analytic continuation from the Matsubara to real frequency domain the development of more reliable tools that are absent of fitting parameters is desirable.

Recently, a procedure for analytic continuation of $G_\sigma(i\omega_n)$ to real frequencies was proposed by Yoon *et al.* [13] on the basis of a machine learning (ML) approach. The authors first generated arbitrary spectral functions $A_\sigma^{\mathrm{training}}(\omega)$ out of approximately 10^5 different configurations classified by number of peaks, their height and their position. Since computing $G_\sigma(i\omega_n)$ for a given $A_\sigma(\omega)$ is straightforward, for supervised ML $G_\sigma^{\mathrm{training}}(i\omega_n)$ was calculated from:

$$G_\sigma^{\mathrm{training}}(i\omega_n) = \int d\omega \frac{A_\sigma^{\mathrm{training}}(\omega)}{i\omega_n - \omega}. \qquad (1)$$

Next, $G_\sigma^{\mathrm{training}}(i\omega_n)$ and $A_\sigma^{\mathrm{training}}(\omega)$ were employed as input and output training datasets in the ML process, respectively. $A_\sigma^{\mathrm{ML}}(\omega)$ was then estimated by the trained parameters of the supervised ML where $G_\sigma(i\omega_n)$ are the input data. The advantage of this ML approach is the absence of a fitting parameter, unlike the case of the maxEn approach. On the other hand, the results are strongly biased by the configurations of the selected training datasets $A_\sigma^{\mathrm{training}}(\omega)$.

In this Letter we suggest an alternative analytic continuation based on a combination of a machine learning (AC+ML) approach with DMFT data extracted from iterative perturbation theory [14–16] (IPT+DMFT) where quantities are obtained in Matsubara and real frequency domains simultaneously. This combined method ensures the absence of a fitting parameter present in the maxEn method and systematically makes the ML training datasets without possible biasing originating from the selections of the training datasets. Moreover, our AC+ML approach directly performs the analytic
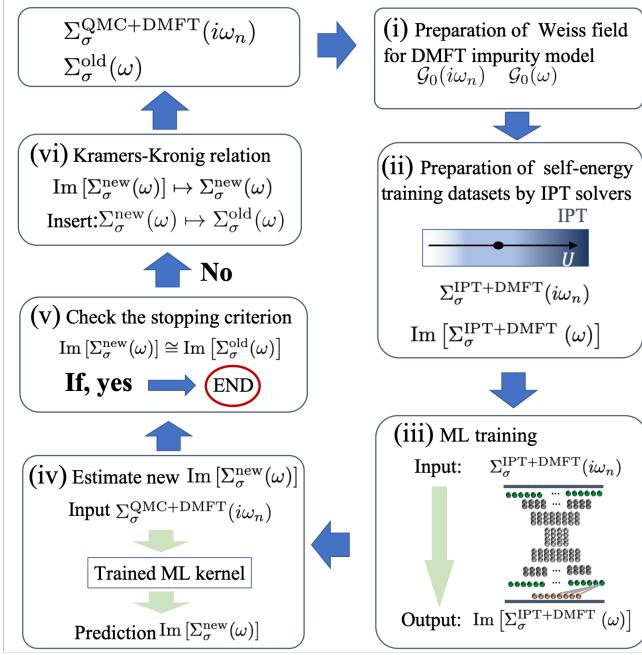
FIG. 1. (Color online) Schematic architecture of the analytic continuation in combination with the machine learning (AC+ML) method. 'IPT' and 'DMFT' denote iterative perturbation theory impurity solver and dynamical mean field theory approximation, respectively. The AC+MC simulation begins in (i) with converged self-energy $\Sigma_\sigma^{\mathrm{QMC+DMFT}}(i\omega_n)$ data and unknown self-energy $\Sigma_\sigma^{\mathrm{old}}(\omega)$. Initially, $\Sigma_\sigma^{\mathrm{old}}(\omega)$ are set to zero in all real frequencies. The input and output training datasets for machine learning (ML) are simultaneously determined by IPT+DMFT on, respectively, Matsubara and real frequency domains in (i) and (ii). The QMC+DMFT self-energy at real frequencies is computed by the trained ML parameters based on convolutional autoencoder tool (iii) and (noisy) input $\Sigma_\sigma^{\mathrm{QMC+DMFT}}(i\omega_n)$ in (iv). When the condition of $\mathrm{Im}[\Sigma_\sigma^{\mathrm{new}}(\omega)] \approx \mathrm{Im}[\Sigma_\sigma^{\mathrm{old}}(\omega)]$ in (v) is satisfied, the patterns of the AC+ML self-energy $\Sigma_\sigma^{\mathrm{AC+ML}}(\omega)$ on real frequencies are fully rearranged, otherwise a new full self-energy is computed by the Kramers-Kronig relation in (vi) and the complete process is repeated. The convergence of the AC+ML method is done within several iterations.

continuation of the converged QMC+DMFT self-energy $\Sigma_\sigma^{\mathrm{QMC+DMFT}}(i\omega_n)$ to real frequencies. We present results for the frustrated Hubbard model on the square lattice and demonstrate the efficiency of the method.

Analytic continuation based on Machine learning.- The idea of the AC+ML method is the following; we take notice of the IPT+DMFT method to make training datasets for the ML process. With IPT+DMFT self-energies can be calculated in both Matsubara and real frequencies at the same time. The method is known to capture various phases such as Fermi-liquid, Mott insulator and the Mott transition, as observed in correlated electronic systems [14–16]. The ML kernel is then constructed from unbiased input datasets $\Sigma_\sigma^{\mathrm{IPT+DMFT}}(i\omega_n)$ and output datasets $\Sigma_\sigma^{\mathrm{IPT+DMFT}}(\omega)$, prepared by the

IPT+DMFT self-consistent equation. The AC+ML self-energy $\Sigma_\sigma^{\mathrm{AC+ML}}(\omega)$ in the real domain is predicted by the trained ML parameters based on a convolutional autoencoder tool [17–20] and input QMC+DMFT self-energy data $\Sigma_\sigma^{\mathrm{QMC+DMFT}}(i\omega_n)$ on the Matsubara domain.

The DMFT self-consistent equation for the real frequency-dependent Green's function can be expressed as

$$G_\sigma(\omega) = \sum_k \frac{1}{\omega + i\delta - \epsilon_k + \mu - \Sigma_\sigma(\omega)}, \qquad (2)$$

where δ, μ and ϵ_k are the broadening factor, chemical potential and energy dispersion, respectively [3]. The DMFT self-consistent equation in the Matsubara domain is identically given as Eq. (2), where $\omega + i\delta$ is replaced by $i\omega_n$.

In Fig. 1 we display the workflow of the simulation procedure of the AC+ML approach. We start with (i) the calculation of the DMFT Weiss fields $\mathcal{G}_0(i\omega_n)$ and $\mathcal{G}_0(\omega)$ with IPT in order to compose the training datasets of ML. For that we consider Eq. (2) and the Dyson's equation, and include the unknown self-energy $\Sigma_\sigma^{\mathrm{old}}(\omega)$ in real frequencies. The unknown self-energy $\Sigma_\sigma^{\mathrm{old}}(\omega)$ are initially set to zero for all frequencies. We also multiply $\Sigma_\sigma^{\mathrm{old}}(\omega)$ by γ to make more configurations for ML, where γ are real numbers larger than one. When $\gamma\Sigma_\sigma^{\mathrm{old}}(\omega)$ are employed in Eq. (2), more new configurations for ML are composed. As the number of values γ is increased, both accuracy of analytic continuation and computational expense increase. In a next step (ii) IPT+DMFT self-energies $\Sigma_\sigma^{\mathrm{IPT+DMFT}}(i\omega_n)$ and $\Sigma_\sigma^{\mathrm{IPT+DMFT}}(\omega)$ with a few hundreds of different configurations are calculated by Eq. (3) given below for input and output training datasets, respectively. In step (iii) the ML parameters are determined by the training input datasets of $\Sigma_\sigma^{\mathrm{IPT+DMFT}}(i\omega_n)$ and output datasets of the imaginary-part of self-energy $\mathrm{Im}[\Sigma_\sigma^{\mathrm{IPT+DMFT}}(\omega)]$ via a one dimensional convolutional autoencoder in Tensorflow-gpu [17–20]. After this, in step (iv) the new imaginary-part of the self-energy $\mathrm{Im}[\Sigma_\sigma^{\mathrm{new}}(\omega)]$ is estimated by the trained ML parameters with input data $\Sigma_\sigma^{\mathrm{QMC+DMFT}}(i\omega_n)$ in Matsubara frequencies. In a next step (v), if the condition of $\mathrm{Im}[\Sigma_\sigma^{\mathrm{new}}(\omega)] \approx \mathrm{Im}[\Sigma_\sigma^{\mathrm{old}}(\omega)]$ is satisfied, the AC+ML simulation is over. Otherwise, after a new full self-energy $\Sigma_\sigma^{\mathrm{new}}(\omega)$ is computed by the Kramers-Kronig relation, it is inserted into Eq. (2) as $\Sigma_\sigma^{\mathrm{old}}(\omega)$, and the AC+ML simulation is repeated again. In most cases the convergence of the AC+ML is done within several iterations.

For the ML process of Fig. 1, as mentioned above, we use a convolutional autoencoder based on stochastic variational Bayes [21–23] with gradient-based optimization [24]. The architecture of our ML kernel consists of encoder, decoder, and fully connected layer. Compared to a previous architecture [23], we use additional channels for dealing with both real- and imaginary-parts of
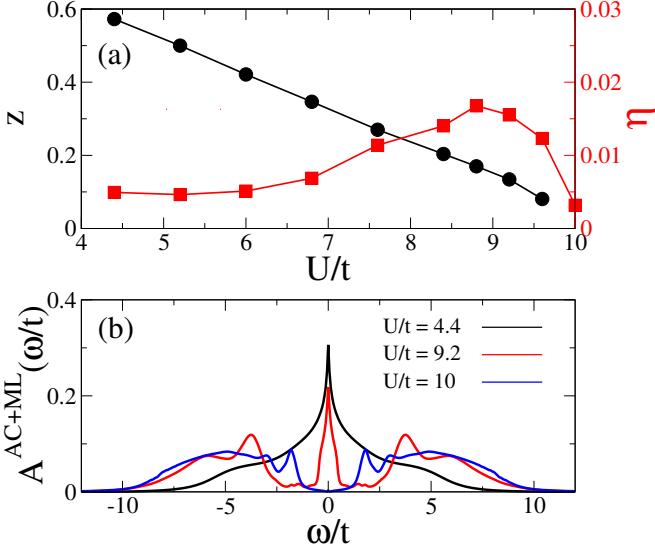
FIG. 2. (Color online) (a) (Left) Quasiparticle weight Z and (Right) η as a function of U/t for temperature $T/t = 0.05$. η is defined as $\eta = \frac{1}{\beta} \sum_{\omega_n} |(G_\sigma^{\mathrm{QMC+DMFT}}(i\omega_n) - G_\sigma^{\mathrm{AC+ML}}(i\omega_n)|$, where $G_\sigma^{\mathrm{AC+ML}}(i\omega_n)$ are recovered by Eq. (1). (b) Spectral function $A_\sigma^{\mathrm{AC+ML}}(\omega)$ for several U/t. All results are obtained from the AC+ML procedure starting with the converged QMC+DMFT self-energy $\Sigma\sigma^{\mathrm{QMC+DMFT}}(i\omega_n)$ on the square lattice at half filling with $t'/t = 0.0$ and $\mu = 0.0$.

$\Sigma_\sigma^{\mathrm{DMFT+QMC}}(i\omega_n)$ input datasets. We employ $i\omega_{n_{\max}}$ input nodes, where $i\omega_{n_{\max}}$ means the maximum number of Matsubara frequencies in $\Sigma_\sigma^{\mathrm{DMFT+QMC}}(i\omega_n)$. The output of the decoder is connected with a single fully connected layer which consists of $\omega_{\max}$ nodes, where $\omega_{\max}$ is the number of real frequencies in $\mathrm{Im}[\Sigma_\sigma^{\mathrm{new}}(\omega)]$.

The IPT+DMFT self-energy on the real domain in (ii) of Fig. 1 is computed by

$$\Sigma_\sigma(\omega) = -U^2 \int d\nu d\nu' d\nu'' \frac{A^{\mathrm{L}}(\nu, \nu', \nu'') + A^{\mathrm{R}}(\nu, \nu', \nu'')}{\omega - \nu + \nu' - \nu''},$$
$$(3)$$

where $A^{\mathrm{L}}(\nu, \nu', \nu'')$ and $A^{\mathrm{R}}(\nu, \nu', \nu'')$ denote $A^-(\nu)A^+(\nu')A^-(\nu'')$ and $A^+(\nu)A^-(\nu')A^+(\nu'')$, respectively. Here, $A^+(\nu)$ and $A^-(\nu)$ are $f(\nu)A(\nu)$ and $f(-\nu)A(\nu)$ respectively, where $f(\nu)$ is the Fermi function expressed in real frequencies ν and $A(\nu)$ is the spectral function at frequency ν. The sum rules of $\mathrm{Im}[\Sigma_\sigma^{\mathrm{new}}(\omega)]$ in (iv) of Fig. 1 are also conserved by

$$\int d\omega \mathrm{Im}[\Sigma_\sigma^{\mathrm{new}}(\omega)] = -\pi U^2 < n_{-\sigma} > (1 - < n_{-\sigma} >),$$
$$(4)$$

where U and $< n_\sigma >$ are the electronic interaction and occupation of electrons, respectively, in the QMC+DMFT calculation. The IPT+DMFT self-energy on the Matsubara domain is identically expressed as Eq. (3), where $\omega + i\delta$ is only replaced into $i\omega_n$.

Results.- In order to test the method, we consider the Hubbard Hamiltonian on the square lattice with

nearest- and next-nearest-neighbor hoppings t and t' respectively in the QMC+DMFT calculations. Then $\epsilon_k = -2t(\cos(k_x) + \cos(k_y)) - 2t'(\cos(k_x + k_y) + \cos(k_x - k_y))$ and the interaction part of the Hamiltonian H_I is given as

$$H_I = U \sum_i (n_{\uparrow,i} - \frac{1}{2})(n_{\downarrow,i} - \frac{1}{2}),$$
$$(5)$$

where $n_{\sigma,i}$ is the number operator at each spin σ and site i. We perform the AC+ML method with the converged QMC+DMFT self-energy $\Sigma\sigma^{\mathrm{QMC+DMFT}}(i\omega_n)$ where we set $\mu = 0.0$. The temperature and the nearest-neighbor hopping strength employed for all QMC+DMFT simulations are $T/t = 0.05$ and $t = 1.0$, respectively. In order to make the ML training datasets in all IPT+DMFT simulations we set $\delta = 0.03$ in Eq. (2).

In Fig. 2 (a) we plot the quasiparticle weight Z defined as $Z = [1 - \frac{\partial \mathrm{Re}\Sigma_\sigma^{\mathrm{AC+ML}}(\omega)}{\partial \omega}|_{\omega=0}]^{-1}$ and the parameter $\eta = \frac{1}{\beta} \sum_{\omega_n} |(G_\sigma^{\mathrm{QMC+DMFT}}(i\omega_n) - G_\sigma^{\mathrm{AC+ML}}(i\omega_n)|$ as a function of U/t for the half-filled case first for $t'/t = 0.0$ and $\mu = 0.0$. η provides an estimate of the deviation of the AC+ML results from the original data in the Matsubara domain. The values of γ used in the IPT+DMFT self-consistent process to make ML training configurations are 1.0, 1.2, 1.4, and 1.6. Here $G_\sigma^{\mathrm{AC+ML}}(i\omega_n)$ is recovered by making use of Eq. (1) via the spectral function. We observe that Z decreases with increasing U/t, corroborating many former results [3, 9]. We identify the Fermi liquid to Mott insulator transition around $U/t = 9.8$. The parameter η mostly increases with increasing of U/t in the Fermi liquid regions. Note that the accuracy of the analytic continuation can be improved with increasing number of γ values.

Fig. 2 (b) displays the spectral function $A_\sigma^{\mathrm{AC+ML}}(\omega)$ for several U/t. $A_\sigma^{\mathrm{AC+ML}}(\omega)$ is determined by

$$A_\sigma^{\mathrm{AC+ML}}(\omega) = -\frac{1}{\pi} \mathrm{Im}[G_\sigma^{\mathrm{AC+ML}}(\omega)],$$
$$(6)$$

where $G_\sigma^{\mathrm{AC+ML}}(\omega)$ has been computed from Eq. (2) with $\Sigma_\sigma^{\mathrm{AC+ML}}(\omega)$. As we expect, the quasiparticle peak at the Fermi level ($\omega = 0$) decreases with increasing U/t in the metallic regimes. The lower and upper Hubbard bands appear at large U/t and the Mott gap is visible at $U/t = 10.0$.

In the following we consider the frustrated Hubbard model [25] with $t'/t = 1.0$ and $\mu = 0.0$. The uncertainty of the analytic continuation in the frustrated system is much larger than that in the half-filled particle-hole symmetric system with $t'/t = 0.0$ because the real-part of the self-energy $\mathrm{Re}[\Sigma_\sigma(i\omega_n)]$ displays charge fluctuations in the QMC+DMFT calculations. Here, we also tune μ to include more training datasets for charge fluctuations in the IPT+DMFT self-consistent process. In order to confirm that our AC+ML approach is working well, in Fig. 3 we plot real- and imaginary-parts of the Green's
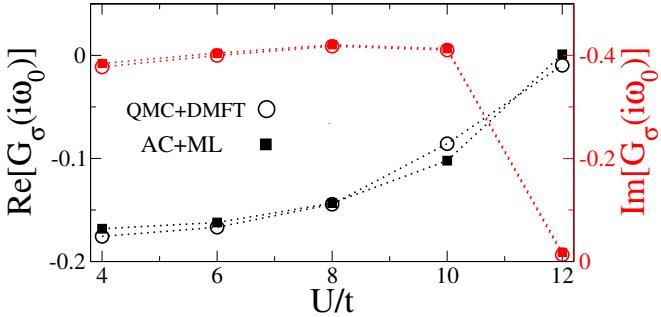
FIG. 3. (Color online) (Left) Real-part of the Green's function $\mathrm{Re}[G_\sigma(i\omega_0)]$ and (Right) imaginary-part of the Green's function $\mathrm{Im}[G_\sigma(i\omega_0)]$ at the first Matsubara frequency $i\omega_0$ as a function of U/t. The results are determined by the AC+ML method of the converged QMC+DMFT self-energy $\Sigma\sigma^{\mathrm{QMC+DMFT}}(i\omega_n)$ for the fully frustrated Hubbard model with $t'/t = 1.0$ and $\mu = 0.0$ on the square lattice.

function at the first Matsubara frequency $i\omega_0$ as a function of U/t in both AC+ML and original QMC+DMFT cases. We find that both results are in an excellent agreement.

We now present in Figs. 4 (a)-(c) the electronic structure $A_\sigma^{\mathrm{AC+ML}}(\omega, k)$ and density of states $A_\sigma^{\mathrm{AC+ML}}(\omega)$ for several U/t values. While the van Hove singularities are clearly seen in the metallic states with $U/t = 8.0$, as in the case of the non-interacting system, the Hubbard bands emerging from electronic correlations are vaguely present around $\omega/t = \pm 5.0$. As U/t increases, the position of the van Hove singularity moves towards $\omega = 0.0$ and there is a transfer of spectral weight towards the upper and lower Hubbard band. At $U/t = 12.0$ the system is a Mott insulator.

Conclusions.- We have proposed a novel analytic continuation AC+ML technique in combination with IPT+DMFT that provides the self-energy $\Sigma\sigma^{\mathrm{QMC+DMFT}}(\omega)$ from $\Sigma\sigma^{\mathrm{QMC+DMFT}}(i\omega_n)$. The trained parameters for ML are determined from input and output training datasets calculated simultaneously by IPT+DMFT on Matsubara and real frequency domains, respectively. The self-energy on the real frequency is obtained from the ML process with (noisy) input QMC+DMFT self-energies in the Matsubara domain and the trained ML parameters based on the convolutional autoencoder approach in each IPT+DMFT self-consistent step. When IPT+DMFT self-consistency including the ML process is completely satisfied, the patterns of QMC+DMFT self-energy on real frequency are rearranged. We demonstrated the powerfulness of the method for the case of the fully frustrated Hubbard model on the square lattice where the QMC+DMFT data in the Matsubara domain are very noisy, and with the proposed method we were able to obtain trustable results at real frequencies.
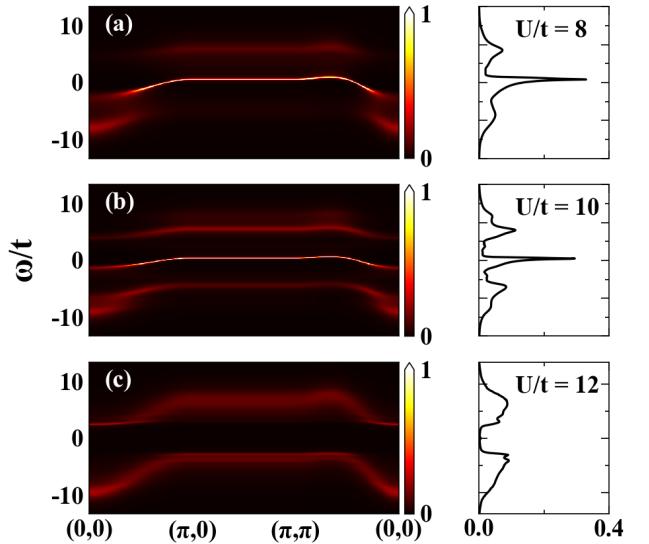
Even though our AC+ML approach is computation-

FIG. 4. (Color online) (Left) Electronic structures $A_\sigma^{\mathrm{AC+ML}}(\omega, k)$ and (Right) $A_\sigma^{\mathrm{AC+ML}}(\omega)$ for (a) $U/t = 8.0$, (b) 10.0, and (c) 12.0. The results are determined by the AC+ML method of the converged QMC+DMFT self-energy $\Sigma\sigma^{\mathrm{QMC+DMFT}}(i\omega_n)$ for the fully frustrated Hubbard model with $t'/t = 1.0$ and $\mu = 0.0$ on the square lattice.

ally more expensive than the maxEn method, it is not only free from bias from selections of ML training datasets and fitting parameters present in the maxEn method, but it directly performs analytic continuation of $\Sigma\sigma^{\mathrm{QMC+DMFT}}(i\omega_n)$ as well, which can be compared with experimental results. Therefore, we believe that our AC+ML method will be useful to investigate electronic properties of correlated systems which require reliable estimates of self-energies and spectral functions in the real frequency domain.

* Email: hplee@kangwon.ac.kr

[1] W. Metzner and D. Vollhardt, Phys. Rev. Lett. **62**, 324 (1989).

[2] A. Georges and G. Kotliar, Phys. Rev. B **45**, 6479 (1992).

[3] A. Georges, G. Kotliar, W. Krauth, and M.J. Rozenberg, Rev. Mod. Phys. **68**, 13 (1996).

[4] G. Kotliar and D. Vollhardt, Physics Today **57**, 53 (2004).

[5] K. Held, Adv. Phys. 56, 829 (2007).

[6] A. N. Rubtsov, V. V. Savkin, and A. I. Lichtenstein, Phys. Rev. B **72**, 035122 (2005).

[7] P. Werner, A. Comanac, L. d. Medici, M. Troyer, and A. J. Millis, Phys. Rev. Lett. **97**, 076405 (2006).

[8] E. Gull, A. J. Millis, A. I. Lichtenstein, A. N. Rubtsov, M. Troyer, and P. Werner, Rev. Mod. Phys. **83**, 349 (2011).

[9] M. Imada, A. Fujimori, Y. Tokura, Rev. Mod. Phys. **70**, 1039 (1998).

[10] G. Kotliar, S. Y. Savrasov, K. Haule, V. S. Oudovenko, O. Parcollet, and C. A. Marianetti, Rev. Mod. Phys. **78**, 865 (2006).

[11] M. Jarrell and J. E. Gubernatis, Physics Reports **269**, 133 (1996).

[12] X. Wang, E. Gull, L. d. Medici, M. Capone, and A. J. Millis, Phys. Rev. B **80**, 045101 (2009).

[13] H. Yoon, J.-H. Sim, and M. J. Han Phys. Rev. B **98**, 245101 (2018).

[14] H. Kajueter and G. Kotliar, Phys. Rev. Lett. **77**, 131 (1996).

[15] L.-F. Arsenault, P. Semon, and A.-M. S. Tremblay, Phys. Rev. B **86**, 085133 (2012).

[16] T. Fujiwara, S. Yamamoto, Y. Ishii, J. Phys. Soc. Jpn **72**, 777 (2003).

[17] Y. LeCun, Y. Bengio, and G. Hinton, Nature **521**, 436 (2015).

[18] I. Goodfellow, Y. Bengio, and A. Courville, Deep Learning (The MIT Press, Cambridge, Massachusetts, 2016).

[19] A. Krizhevsky, I. Sutskever, G. E. Hinton, Advances in neural information processing systems, 1097 (2012).

[20] M. Abadi et al., TensorFlow: Large-scale machine learning on heterogeneous systems, 2015. Software available from https://www.tensorflow.org/.

[21] Y. Bengio, A. Courville, and P. Vincent, arXiv:1206.5538 (2014).

[22] D. P. Kingma, and M. Welling, arXiv:1312.6114 (2013).

[23] T. Song and H. Lee, Phys. Rev. B **100**, 045153 (2019).

[24] D. P. Kingma and J. Ba, arXiv:1412.6980 (2014).

[25] L. F. Tocchio, H. Lee, H. O. Jeschke, R. Valentí, C. Gros Phys. Rev. B **87**, 045111 (2013).